PROJECTILE PENETRATION INTO REINFORCED CONCRETE: ANALYSIS OF INTERACTION AND ITS EXPERIMENTAL VERIFICATION

M. M. Conrad

RUAG Land Systems, Warhead Division, Allmendstrasse 86, CH–3602 Thun, Switzerland
email: markus.conrad@ruag.com

1. SUMMARY

This is a study of the physical penetration of reinforced concrete (thickness 20 and 25cm) by a rod shaped penetrator (ratio length/diameter = 6—11) in the impact velocity range 175—250m/s. The inclining of the target is between 0° and 35°. A computational constitutive model for concrete will be validated by experiments. The numerical simulation predicts rather accurately the penetration depth, exit velocity, ricochet as well as mechanical behaviour in stress and failure of the penetrator.

2. INTRODUCTION

Concrete is a brittle composite material with distinct behaviour in dilatation and compression. In addition, the strength of the concrete diminishes, especially after tensile loading, so that the original strength is never reached again. T. J. Holmquist *et al.* 1,2 take this fact into consideration by introducing a damage parameter, similar to the Johnson-Cook fracture model. The T.J. Holmquist fracture model accumulates damage from both equivalent plastic strain and plastic volumetric strain. The increase in damage reduces the yield strength. W. Riedel 3 completed the model by considering strain hardening. In addition, the yield stress depends on the triaxial direction of the stress load. A continuous transition from ductile behaviour of compressed zones to brittle behaviour of expanding zones in tension is proposed by transforming the von Mises yield surface (ductile) into Rankine's yield surface (brittle) following to William and Warnke 4. Thus, the yield strength reduces from an upper value for triaxial pressure to a lower value for triaxial tension. However, the yield strength may increase if the stress loading moves toward triaxial pressure. A sophisticated damage model of B.J. Thorne 5 is based on the assumption that the material is permeated by an array of randomly distributed and orientated micro cracks. Crack formation and growth are combined in one damage parameter.

The present constitutive model for finite difference computer codes unifies all these features by following combination: The damage parameter increases following both the model of T. J. Holmquist *et al.* 1 for zones with compression and the model of B. J. Thorne 5 for zones with dilatation. The yield strength is not a

function of the triaxial stress load direction, in order not to consider the effects of tensional load to the yield strength reduction twice. It has become apparent that the damage of Thorne's model grows extremely fast in comparison with the damage of Holmquist's model. However, strain hardening effects are considered as proposed by W. Riedel 3. In addition, the bulk modulus is a function of damage as proposed by Hashin's theory 6. This should only influence hydrostatic tensile stresses, because the Hugoniot curve for hydrostatic pressure is based on experimental results, and thus, the damage is already included in the Hugoniot curve. The combined material model, whose parameter values are taken from the literature, will be validated by a variety of long rod penetrators impacting different reinforced concrete walls.

3. CONSTITUTIVE MODEL FOR CONCRETE

Equation of state

The stress load s is decomposed into a hydrostatic pressure p and deviatory stress σ: $s = p + \sigma$. The pressure is a function of compression $\mu = \rho/\rho_0 - 1$, with ρ_0 and ρ the initial and updated density respectively. The Hugoniot curve is given in 9; essential values are summarised in Table 1.

Table I

Hugoniot curve data for initial loading (left) and crushing (right). T–maximum tensile strength, K–bulk modulus, D–damage parameter (D = 1: fully damaged), μ_E–value of μ, where the curve with slope K intersects the line with constant value 0.0358, μ_{max}–maximum value of μ previously seen by the zone.

Initial loading characteristic		Crushing: unloading and reloading	
Compression μ	Pressure p /GPa/	μ	Pressure p /GPa/
$-\infty$ ... –T (1–D) /K	–T (1–D) /K	$-\infty$ ... μ_E	K μ, i.e. slope = K
–T (1–D) / K ... μ_E	K μ		
μ_E ...0.1	0.0358 +7.862 (μ–μ_E)	μ_E ...0.223	slope: $\left(\frac{(78.4-K)(\mu_{max}-\mu_E)}{(0.223-\mu_E)}+K\right)$
0.1 ... 0.2	0.8 – 13.0 (μ – 0.1)		
0.2 ... 0.3	2.1 – 42.0 (μ – 0.2)	0.223 ... ∞	78.4 (μ – 0.223), i.e. slope = 78.4

The relationship between Damage D, Young's modulus E, bulk modulus K and Poisson's ratio ν is according to Hashin's theory

$$D = \frac{5}{8}\left(\frac{\nu_0}{\nu}\right); \frac{15}{64}\ln\left(\frac{1-\nu}{1-\nu_0}\right)+\frac{45}{128}\ln\left(\frac{1+\nu}{1+\nu_0}\right)+\frac{5}{128}\ln\left(\frac{3-\nu}{3+\nu_0}\right);$$

$$\frac{E}{E_0} = \left(\frac{\nu}{\nu_0}\right)^{10/9}\left(\frac{3-\nu_0}{3+\nu}\right)^{1/9}; K = \frac{E}{3(1-2\nu)}$$

with E_0 and ν_0 the initial Young's modulus and Poisson's ratio respectively. This relationship is only applied to zones with dilatation. The initial Young's modulus is expressed in terms of initial density ρ_0 and the compressive strength f'_c of the concrete according to 9: $E_0 = 33\ \rho_0^{1.5}\ f'^{0.5}_c$.

Yield strength

The dimensionless plastic yield strength $Y^*_{plastic} = Y_{plastic}/f'_c$ is given in 3 according to 1 and 2:

$$Y^*_{plastic} = \left(Y^*_{failure}(1-D)+D\,Y^*_{residual}\right)\left(1+C\ln(\dot{\varepsilon}/1.0)\right) \text{ with } C = \begin{cases} 0.000 & \forall\ \dot{\varepsilon} < 1.0 \\ 0.007 & \forall\ \dot{\varepsilon} > 1.0 \end{cases}$$

$$Y^*_{failure} = B_{failure}\left(\frac{p+T(1-D)}{f'_c}\right)^{0.61}; Y^*_{residual} = B_{residual}\left(\frac{p}{f'_c}\right)^{0.61}; \text{with } \begin{cases} B_{failure} = 1.6 \\ B_{residual} = 1.6 \end{cases}$$

The plastic yield strength has its maximum value at start ($Y^*_{failure}$). The minimum value $Y^*_{residual}$ is achieved with full damage (D=1). However, yielding starts at the elastic surface $Y^*_{elastic}$ defined as:

$$Y^*_{elastic} = \begin{cases} 0.70\,Y^*_{plastic} & \text{dilatation} \\ 0.53\,Y^*_{plastic}\cdot F_{cap} & \text{compression} \end{cases}; F_{cap} = \begin{cases} 1 & \forall \quad p < 0.49\,f'_c \\ \sqrt{1-\left[(p/f'_c-0.49)/(7-0.49)\right]^2} & \forall \quad 0.49\,f'_c < p < 7.0\,f'_c \\ 0 & \forall \quad p > 7.0\,f'_c \end{cases}$$

Strain hardening is determined with the help of the effective plastic strain ε_{effpl} and the elongation limit ε_{max} obtained from a specimen under compressive uniaxial load. W. Riedel derived an interesting relationship between ε_{max} and the shear modulus $G_0=E_0/2(1+\nu_0)$ resulting in a final yield strength:

$$Y_0 = \min\left[Y_{elastic}+\varepsilon_{effpl}\cdot\frac{(Y_{failure}-Y_{elastic})}{\varepsilon_{max}}\,\middle|\,Y_{plastic}\right] \quad \text{with} \quad \frac{(Y_{failure}-Y_{elastic})}{\varepsilon_{max}} \approx 3\cdot G_0$$

Damage parameter

T.J. Holmquist *et al.* 1 postulate that the damage increment ΔD is connected to the increments of both, plastic strain $\Delta\varepsilon_{effpl}$ and volumetric plastic strain $\Delta\mu_{crush}$. Damage D is accumulated from the increments only if the accumulated plastic strain exceeds a minimum value:

$$\Delta D = \frac{|\Delta\varepsilon_{effpl}| + |\Delta\mu_{crush}|}{\varepsilon_p^{failure} + \mu_p^{failure}} \quad ; \quad \varepsilon_p^{failure} + \mu_p^{failure} = 0.04\left(\frac{p}{f'_c} + \frac{T}{f'_c}\right)^{1.0} \quad ; \quad D = \begin{cases} 0 & \forall \sum|\Delta\varepsilon_{effpl}| < 0.01 \\ \sum \Delta D & \forall \sum|\Delta\varepsilon_{effpl}| \geq 0.01 \end{cases}$$

This model delivers good results for zones with compression. When the material is expanding in tension, the damage model of B.J. Thorne 5 is applied. The damage increment ΔD is a function of fracture toughness K_{IC}, initial density ρ_0, initial sound velocity c_0, the damage dependent bulk modulus K, damage dependent Poisson's ratio ν, maximum previous strain rate $\dot{\varepsilon}_{max}$, and volumetric strain μ:

$$\Delta D = \left| \frac{5\,k\,m\,\mu^{m-1}}{2} \underbrace{\left(\frac{K_{IC}}{\rho_0 c_0 \dot{\varepsilon}_{max}}\right)^2}_{\text{term II}} \Delta\mu \right| \quad ; \quad k = \frac{1-2\nu}{(1-\nu^2)(1+\nu)} k_0 \; ; k_0 = \frac{29.4\,N_s^4}{\pi}\left(\frac{K}{K_{IC}}\right)^6\left(\frac{1}{2(1+\nu)}\right)^2$$

The idea is that a description of the number of cracks is given by a Weibull distribution form $k\mu^m$, with Weibull exponent m=6 and a factor k given above. The term II stems from a nominal fragment radius derived from energy consideration on a uniformly expanding sphere. The factor k_0 is based on a reasonable relation between maximum tensile strength and the strain rate for rocks with penny shaped flaws N_s=1.12. To assure that unreasonable small values of $\dot{\varepsilon}_{max}$ are not used in the equations above, a material dependent minimum significant strain rate $\dot{\varepsilon}_{min}$ is used until $\dot{\varepsilon}$ exceeds $\dot{\varepsilon}_{min} \approx$ 20—1000/s. It has to be emphasised that a measure of the *probability* of fracture at given strain rate and accumulated volumetric plastic strain has been derived with the help of Weibull statistics.

Material input values

Precise numerical predictions have been obtained with the following material input values:

strength f'_c	density ρ_0	frac. toughness K_{IC}	max. tens. strength T	ν_0	$\dot{\varepsilon}_{min}$	total failure criteria
48MPa	2440kg/m^3	1.68MPa $\sqrt{m}$	4MPa	0.22	100/s	$\varepsilon_{effpl} > 2.0$

4. EXPERIMENTS

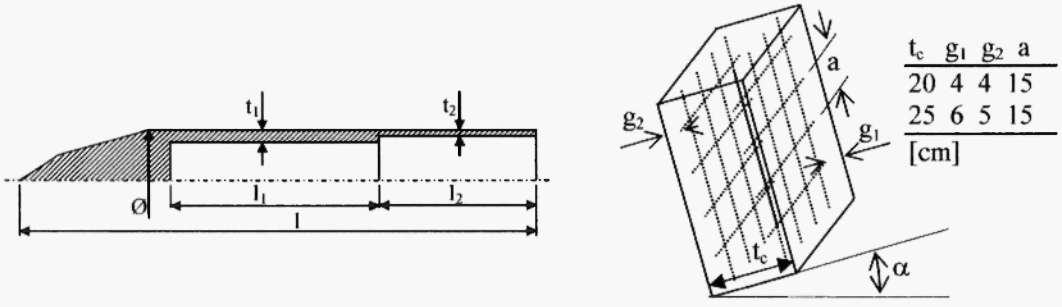

Fig. 1: Penetrator with double cone nose; dimensions are given in Table 2. Concrete target with obliquity α: Two different targets have been used (thickness 20 and 25cm) whose characteristics are listed in the table on the upper right. The dimensions of the faces are 1.2m × 1.0m. Reinforcement is realised with two meshes of steel St37 rebar Ø 9mm with distance g_1 and g_2 from the impact and opposite face respectively. The mesh size is a =15cm.

An overview of all impact experiments (7 different types of penetrators and two different concrete targets) is given in Fig. 1 and Table 2. The hollow penetrators have either been filled with high explosive (#1–5 and #13–15) or an acceleration unit, i.e. battery and processor with 140kHz sampling rate, has been placed in the drill hole (#11&12). In some experiments (#6–10) solid monobloc penetrators have been used. Whenever the target has been perforated one is interested where the penetrator has been found. Otherwise, the penetration depth has been measured.

Table 2

Overview of the experiments, target and penetrator geometries (cp. Fig. 1). The targets of test #1–3, 5–7, 9, 11, 14 have been perforated. The last two columns show either the penetration depth or the velocity of the penetrator whose double cone nose has just completely passed the back surface of the concrete target. However, deceleration continues due to the friction between the shell of the penetrator and the perforated concrete. Test #2, 3, 4–7, 9, and 14 have been performed around the limit impact velocity v needed for perforation.

#	t_c	α	v	mass	Ø	l	l_1	t_1	l_2	t_2	Result	Simulation	
	[cm]	[°]	[m/s]	[kg]	[mm]							[cm]	[m/s]
1	20	2.5	220	2.05	34	329	186	5.5	60	3.5			10
2		2.5	214								25m behind target		5
3		2.0	176								just behind target	16.7	-3
4		4.5	251	0.78	32	214	83	4.5	60	2.5	penetration 10.0cm	13.0	
5											penetrator got stuck		

Table 2 (continued)

6	25	1.1	208	2.05	32	347	solid				18m behind target		15
7		2.5	217		38	259					just behind target		22
8		7.3	178								penetration 14.5cm	15.5	
9		24.8	225								8m behind target		10
10		30.0	229								penetration 12.5cm	14.0	
11	20	5.0	214	1.99	34	330	105	4.5	90	3.0	accelerometer	Fig. 4 left	
12		6.2	248	1.08	33			4.0		2.0	penetrator broken	Fig. 4 right	
13		35	242	2.05	34	329	186	5.5	60	3.5	ricochet 9.5cm	10.0	
14		22.8	232	1.37	30	330	205	6.5	52	4.0	just behind target	18.7	0
15		30									penetration 9.0 cm	14.0	
	main parameters for perforation → response in penetrator												

5. RESULTS

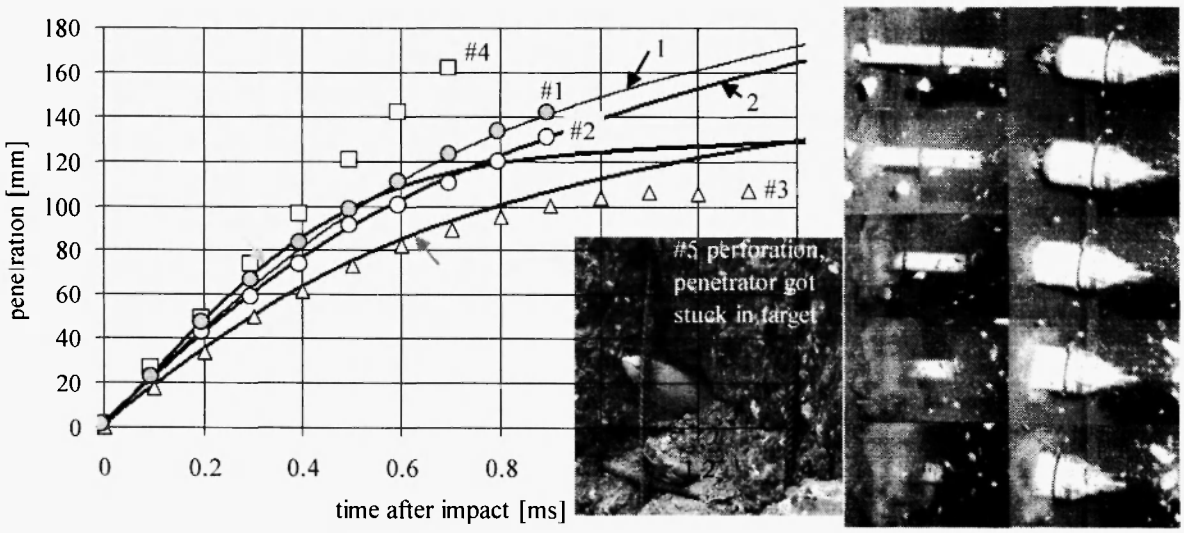

Fig. 2: Measurements of the penetration depth of test #1–5 (see Table 2) in comparison to computational prediction (left). The depth has been measured from a sequence of frames obtained from a ultra high speed camera as shown on the right hand side for test #2 at 100, 300, 500, 700, and 900 microseconds and test #4 at -50, 50, 150, 250, and 350 microseconds after impact. The penetrator of test #4 has been placed inside a body (cp. fig. 4).

Fig. 2 compares computational predictions with measurements of test #1–5. It is interesting that in test #4 the target has not been perforated whereas in #5 the penetrator got stuck as shown in Fig. 2, even though the initial conditions were the same. This difference is due to some statistical effects of the concrete (see section "Damage parameter"). However, the exact position of the impact with respect to the rebars (especially for the face opposite to the impact) may also be decisive for perforation. For tests #3 and #14, the penetrator was found just behind the target. The computation predicts a penetration depth of 16.7 and 18.7cm, i.e. the tip if the penetrator has just passed the second reinforcement mesh (at a distance of 4cm from the back face of the target, see g_2 in Fig. 1). Perforation is probable, because big chunks of concrete have been broken out from the back face.

The measured points on test #4 are on a straight line, because the penetrator has been placed inside a body, so that only the nose of the penetrator is visible on the frames (Fig. 2, on the right hand side). The mechanism is visible on Fig. 4: After failure of a predetermined breaking point (150μs after impact) the penetrator flies detached from the body. However, 400μs after impact, the end of the penetrator is strongly pushed forward, so that the breakage happens in the mid part of the penetrator, i.e. in the transition zone, where the thickness is reduced in a single step from 4mm to 2mm. In test #13, breakage has occurred in a zone between 14.5cm and 19cm behind the tip of the penetrator, whereas the corresponding result of a rough simulation is between 17 and 20cm.

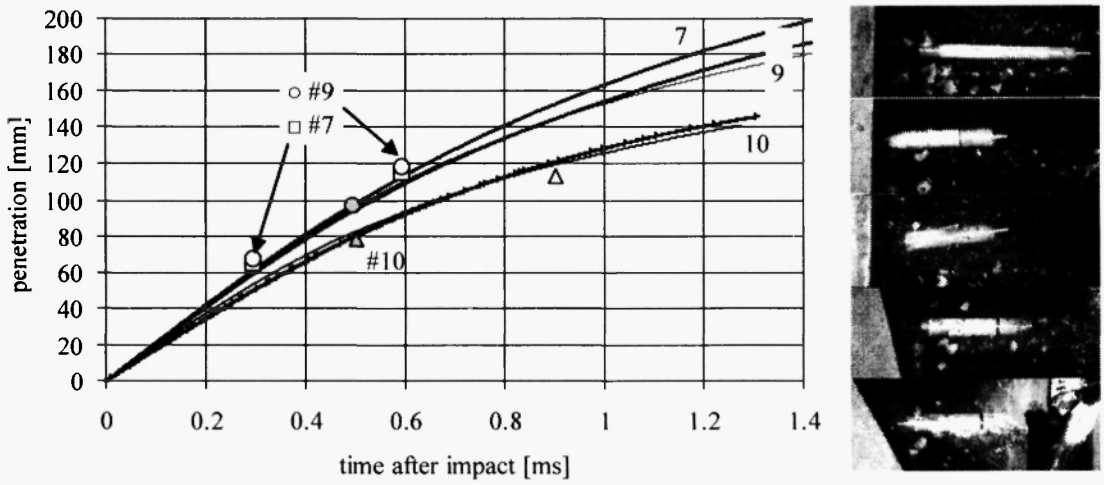

Fig. 3: Measurement of the penetration depth of test #6–10 in comparison to computational result. The depth has been measured with the help of triple exposures (test #6–10 from top to bottom on the right hand side) as indicated by the arrows.

During the perforation, the penetrator oscillates. Therefore, the acceleration unit of test #11 returned peak values exceeding the mean values (see Fig. 4 top). However, the supporting of the acceleration unit inside the penetrator has some damping behaviour resulting in a low pass filter frequency around 15kHz. Thus the thin

line (filter frequency 10kHz) is nearly coincident with the dotted line (filter frequency 15kHz). The corresponding simulation (Fig. 4 bottom) shows different behaviour, since the response in the penetrator itself has been evaluated rather than the response in the acceleration unit. Consequently, the simulation returns also high frequency oscillations. Because of the unknown transfer function between penetrator and acceleration unit only a qualitative comparison is given.

Influence of the rebars:

Experiments as simulations clearly showed that the perforation is hardly affected when the penetrator directly hits a rebar near the surface of the impact, because the yield strength of St37 is in the order of the magnitude of the computed yield strength Y_0. However, a rebar on the back surface has some influence, because of the strongly reduced velocity of the penetrator, so that the resistance inside the concrete is rather low compared to the resistance of St37. In addition, the stress distribution is "guided" by the rebars as shown in Fig. 4 on the right hand side. Especially the rebars near the back surface smear out the load, so that the area involved in penetration resistance grows. Consequently, local high stresses leading to erosion are reduced.

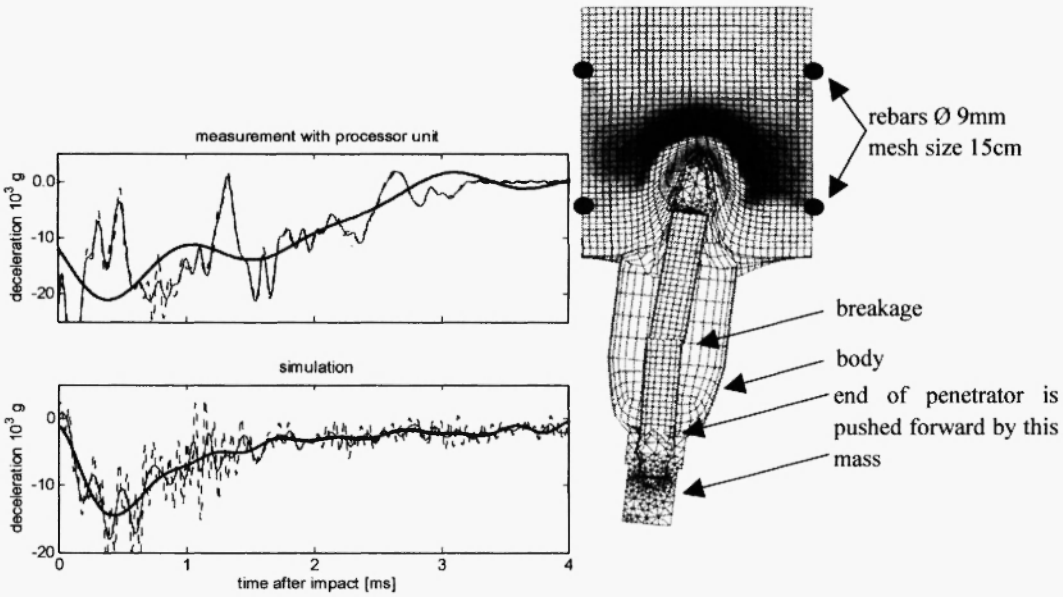

Fig. 4: Deceleration history of test #11 (top) in comparison with computation (bottom) filtered by a low pass filter with filter frequency at 1 and 2 kHz respectively (thick lines). Additional low pass filters at 10 kHz (thin lines) and 15kHz (dashed lines) are given for comparison. Effective stress distribution of test #12 in the central part of concrete (Lagrange HEXA Elements with 5mm edge length) and breakage of the penetrator, after its end has been pushed forward by a mass (Lagrange TETRA Elements) fixed to the rear part of the body are shown on the right hand side.

6. CONCLUSIONS

The present finite difference simulation predicts rather accurately the penetration depth and exit velocity. Even ricochet leading to breakage in the mid part of the penetrator is satisfactorily reproduced. Consequently, the resistance to the penetration inside the concrete and the stress response inside the penetrator can be accurately estimated. However, the concrete has some accidental behaviour, so that around the limit impact velocity for perforation the results of repeated experiments are different. This fact is considered in the simulation by Thorn's damage model, which is a measure of the *probability* of fracture inside the concrete.

ACKNOWLEDGMENTS:

All measurements have been done by the Swiss Army Procurement Agency.

7. REFERENCES

1. T.J. Holmquist, G.R. Johnson and W.H. Cook, A Computational Constitutive Model for Concrete Subjected to Large Strain, High Strain Rates, and Pressure, *14th International Symposium on Ballistic*, Québec, Canada, 1993.
2. G.R. Johnson and T.J. Holmquist, *An Improved Computational Constitutive Model for Brittle Materials*, American Institute of Physics, 1994; pp. 981-984.
3. W. Riedel, *Beton unter dynamischen Lasten: Meso- und makromechanische Modelle und ihre Parameter*, Universität der Bundeswehr München, Fraunhofer Institut für Kurzzeitdynamik, Ernst Mach Institut (2000).
4. K.J. William and E.P. Warnke, Constitutive Model for the Triaxial Behaviour of Concrete, International Association of Bridge and Structural Engineers, *Seminar on Concrete Structure Subjected to Triaxial Stresses, IABSE Proc.* 19, Italy, 1975.
5. B.J. Thorne, A Damage Model for Rock Fragmentation and Comparison of Calculations With Blasting Experiments in Granite, *SAND90-1389*, Sandia National Laboratories, Albuquerque NM, (October 1990).
6. Z. Hashin, The Elastic Moduli of Heterogeneous Materials, *Journal of Applied Mechanics, Transaction of ASME*, 50 (1962).
7. V.G. Gregson, *A Shock Wave Study of Fondue-Frye WA-1 and a Concrete*, DNA 2797F, 1972.
8. J. Chinn and R.M. Zimmermann, *Behavior of Plain Concrete Under Various High Triaxial Compression Loading Conditions*, AFWL-TR-64_163, 1968.
9. D.A. Matuska, J.J. Osborn and E.W. Piburn, *HULL Documentation Volume I User Manual*, Orlando Technology, Inc., 60 Second Street, Bldg. 5, Shalimar, FL 32579.